

Synthesis mechanism, enhanced visible-light-photocatalytic properties, and photogenerated hydroxyl radicals of PS@CdS core-shell nanohybrids

Han Wang · Qian Xu · Xing Zheng ·
Wenqing Han · Jingtang Zheng · Bo Jiang ·
Qinzhong Xue · Mingbo Wu

Received: 10 October 2014 / Accepted: 2 December 2014 / Published online: 23 December 2014
© Springer Science+Business Media Dordrecht 2014

Abstract In this study, spherical polystyrene (PS)@CdS core-shell structure nanoparticles (CSNPs) were prepared by sonochemical method. The influences of the surfactant PVP, the order of adding precursors, the molar ratio of S/Cd, and the reaction time on structure were carefully studied. Results of SEM, TEM, EDS, XRD, and FT-IR showed that the as-prepared nanohybrids have a typical core-shell structure with 260 nm core and a uniform shell with thickness ranging from 10 to 30 nm, both PVP and the order of adding precursors were the controlling parameters. In addition, the as-synthesized PS@CdS CSNPs exhibited much higher photocatalytic activity for RhB under visible light irradiation compared with pure CdS, which should be attributed to their synergic

effect between core and shell, amount of hydroxyl groups on the surface, good monodispersity, and so on. Besides, the production of photogenerated hydroxyl radical ($\cdot\text{OH}$) was in accordance with the RhB decolorization efficiency from the prepared PS@CdS CSNPs. It indicated that $\cdot\text{OH}$ was the main active oxygen species in the photocatalytic process.

Keywords CdS · Core-shell structure · Ultrasonic method · Photocatalysis · Hydroxyl radical

Introduction

Among various hybrid materials, core-shell structure nanohybrids comprising a polymer latex covered with a semiconducting nanocrystal shell have received growing attention of scientists due to their hybrid composition, unique arrangement, and the properties of multiple nanoparticles (Caruso 2001; Ghosh Chaudhuri and Paria 2011). In particular, polystyrene-based polymeric colloids containing functional groups have been mostly employed as cores (Imhof 2001; Kim et al. 2006). Uniform and controllable sizes, large surface areas, adsorption capacities, and easy preparations of polymeric colloids make them attractive core and/or template materials in the preparations of colloidal organic@inorganic core-shell nanohybrids including PS@TiO₂ (Karabacak et al. 2014; Shi et al. 2012), PS@Fe₃O₄ (Fang et al. 2009), PS@SiO₂ (Mu and Fu 2012), PS@CdS (Wang et al. 2007, Zhang et al.

H. Wang (✉) · Q. Xu · J. Zheng · B. Jiang ·
Q. Xue · M. Wu

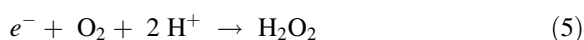
State Key Laboratory of Heavy Oil Processing, China
University of Petroleum, Qingdao 266580, Shandong,
People's Republic of China
e-mail: wanghan960070@126.com

J. Zheng
e-mail: jtzheng03@163.com

H. Wang · W. Han
Baotou Light Industry and Vocational Technical College,
Baotou 014045, People's Republic of China

X. Zheng
Beijing ZNHK Science and Technology Development
Co., LTD, Beijing 100080, People's Republic of China
e-mail: znhk113@163.com

2005), PS@CdTe (Rogach et al. 2000), PS@ZnS (Huang et al. 2007; Yin et al. 2003), etc. Moreover, depending upon the type of conductivity of the shell, they exhibited various properties such as magnetic, electrical, catalytic, and optical, and therefore have extensive potential applications in the fields of medical science, biology, catalysts, coatings, and in many other fields (Coşkun and Korkmaz 2014; Ghosh Chaudhuri and Paria 2011; Radmilovic et al. 2011; Shenoy et al. 2003; Zhang et al. 2010). It has been proved that cadmiumsulfide (CdS) is an important II–VI semiconductor with a narrow band gap of 2.42 eV. It can absorb most of the visible light in the solar spectrum and has potential applications in the electro-optic field (Sanchez et al. 2005). CdS can be evoked by visible light to yield $\bullet\text{OH}$ in photocatalytic reactions (Eqs. 1–6), and $\bullet\text{OH}$ owns high oxidation potentials 2.8 V ($E^0(\bullet\text{OH}/\text{H}_2\text{O})$), which chronologically stages reactions of environmental pollutant macromolecules into smaller and less harmful substances (Rauf and Ashraf 2009). Hence, CdS-mediated photocatalysis has been applied in the degradation of many organic contaminants (Ishibashi et al. 2000a, b).



In order to acquire the enhanced properties or be more suitable for applications, many organic/inorganic@CdS core–shell structures have been fabricated by various techniques, such as layer-by-layer (LBL) (Zhang et al. 2005), chemical method (Monteiro et al. 2002), microwave-assisted method (Hu et al. 2010; Wang et al. 2007), electrostatic self-assembly strategy (Rogach et al. 2000; Sherman and Ford 2005), surface-initiated atom transfer radical polymerization (ATRP) (Wang et al. 2008), thermal decomposition approach (Kandula and Jeevanandam 2014), etc.

Compared with the similar nanostructures synthesized by other methods, the sonochemical method is mild, convenient, inexpensive, green, and efficient.

Furthermore, the chemical reactions in heterogeneous liquid–solid system can be improved and the process of mass transfer can be strengthened by sonochemical method, which makes the system's microcosmic or submicroscopic intimate mixing achievable, as well as the growth of crystal and the agglomeration of particles controllable. Accordingly, ultrafine particles with narrow particle size distribution were obtained (Bang and Suslick 2010). As a result, it has been successfully used to synthesize a variety of nano singles and composite materials including core–shell structure. Currently, lots of core–shell structure nanocomposites have been synthesized by the cavitation of sonochemical synthetic method, e.g., Au@Pd (Mizukoshi et al. 2000), Au@Ag (Anandan et al. 2008), Fe–Ni@iron oxide (Douvalis et al. 2012), Fe_3O_4 @ SiO_2 (Morel et al. 2008), CaCO_3 @ SiO_2 (Virtudazo et al. 2013), CdSe@ZnS (Murcia et al. 2006), ZnO@CdS (Geng et al. 2011), SiO_2 @CdS (Siva et al. 2014), and PS@ZnS (Breen et al. 2001). However, few studies have been reported involving PS@CdS nanoparticles synthesized via the sonochemical method.

In the present study, PS@CdS CSNPs were prepared by the gentle and efficient sonochemical method using cadmium acetate ($\text{Cd}(\text{Ac})_2$) and thioacetamide (TAA) as precursors, PVP as coupling agent, and PS microspheres as template. In order to in-depth understand the formation mechanism of the PS@CdS CSNPs, parameters such as PVP, the order of adding precursors, the molar ratio of S/Cd, as well as the reaction time were examined in detail. The photocatalytic activity of the samples was evaluated by the decoloration of RhB in aqueous solution under visible light irradiation. Under the same irradiation conditions, PS@CdS CSNPs can generate hydroxyl radicals ($\bullet\text{OH}$), which were detected by photoluminescence (PL) spectroscopy using coumarin (COU) as a probe molecule. Additionally, isopropanol was added to the RhB solution to detect the primary active species in the RhB/PS@CdS CSNPs systems; degradation mechanism of RhB over PS@CdS CSNPs was also proposed.

Experimental details

Materials

Styrene, NaHCO_3 , sodium styrene sulfonate ($\text{C}_8\text{H}_7\text{NaO}_3\text{S}$), persulfate ($\text{K}_2\text{S}_2\text{O}_8$), polyvinylpyrrolidone

(PVP, $M_w = 40,000 \text{ g mol}^{-1}$), thioacetamide (TAA, $\text{C}_2\text{H}_5\text{NS}$), cadmium acetate ($\text{Cd}(\text{CH}_3\text{COO})_2 \cdot 2\text{H}_2\text{O}$), rhodamine-B (RhB), coumarin ($\text{C}_9\text{H}_6\text{O}_2$), isopropanol, and ethanol were purchased from Sinopharm Chemical Reagent Co., Ltd, (China). All reagents were analytical grade and used without further purification. Deionized water was made in laboratory.

Preparation of monodisperse polystyrene microspheres

Monodisperse polystyrene microspheres were made via emulsifier-free emulsion polymerization (Li et al. 2007) described as follows: 41.2 mg of sodium styrene sulfonate (SSS) and 128.1 mg of sodium bicarbonate were mixed in 200 mL of deionized water under N_2 atmosphere. Styrene (St) monomer was added quickly when the bath temperature was raised to 70°C . 30 min later, an appropriate amount of potassium persulfate (KPS) as initiator was added. After 28 h, products were collected after cooling.

Preparation of PS@CdS CSNPs

All the reactions were carried out in 53 kHz Ultrasonic Cleaner (Shanghai KUDOS Ultrasonic Instrument Co., Ltd., China, SK3210HP). Typically, 1.2 mL of PS emulsion and 0.2 g of PVP were added in 20 mL of ethanol one after another under sonication for 30 min. Then 100 mL 0.28 mol/L aqueous solution of TAA was added in the above solution. After 30 min, 100 mL of 0.2 mol/L aqueous solution of cadmium acetate was added. After 3 h sonication, PS@CdS CSNPs, a kind of lemon yellow powder, were prepared and collected by centrifugation, washed with deionized water and ethanol, and dried. As a comparison, pure CdS nanoparticles were prepared by the above-mentioned procedures but without PS microspheres.

Measurement and characterization

The Zeta potential (ζ) measurements of the samples were performed by Model PHS-3C pH Meter Instruction Manual (Shanghai Rex Instrument Factory). Microstructural characterizations of the core-shell nanoparticles were carried out by field

emission scanning electron microscopy (FE-SEM, Japan Hitachi Ltd, S4800), and transmission electron microscopy (TEM, Japanese electronics, JEM-2100UHR) operated at an accelerating voltage of 200 kV. Compositional analysis was performed by energy-dispersive X-ray analysis (EDS) combined with FE-SEM. Phase determination of the core-shell nanoparticles was carried out by an X-ray diffractometer (XRD, PANalytical B.V., X'Pert Pro MPD) using Ni-filtered Cu K-alpha radiation at 40 kV and 40 mA in the 2θ range of 20° – 80° , with a scan rate of 0.02° per second (wavelength = 1.54056 \AA). FT-IR spectra of the samples were recorded in the wavenumber range of $4,000$ – 400 cm^{-1} with a Fourier transform infrared spectrophotometer (FT-IR, Thermo Nicole, TNEX-US). UV-Vis diffuse reflectance spectra (UV-Vis DRS) were obtained for the dry-pressed disk samples using a UV-Vis spectrometer (UV-2450, Shimadzu, Japan). BaSO_4 was used as a reflectance standard in UV-Vis diffuse reflectance experiments. All measurements were carried out at room temperature.

Photocatalytic activity measurements

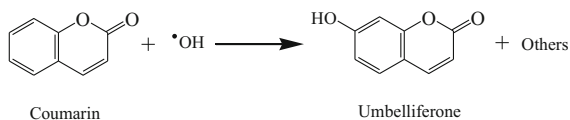
The photocatalytic activity of the PS@CdS CSNPs was evaluated by the decoloration of RhB in aqueous solution under visible light irradiation of a 35-W Xenon arc lamp with a 420 nm cutoff filter. The corresponding focused light intensity on the flask was 360 W/m^2 . In a typical photocatalytic experiment, 100 mL, 10 mg/L RhB ($2 \mu\text{M}$), and 25 mg PS@CdS CSNPs (catalyst loading was 0.25 g/L) were mixed by magnetic stirring for 0.5 h under dark conditions to ensure the establishment of an adsorption/desorption equilibrium between the organics and the catalyst. Then the suspensions were irradiated by visible light. At the given irradiation time intervals, 5 mL solution was sampled and centrifuged, then the clear solution was taken out and its absorbance was recorded by a UV-Vis spectrophotometer (Shanghai Lengguang Technology Co., Ltd., China, GS54T) in the wavelength range 200–800 nm. The decolorization efficiency (η) of RhB was calculated with the following equation (Eq. 7):

$$\eta (\%) = \frac{C_0 - C_t}{C_0} \times 100 \%, \quad (7)$$

where η is the decolorization efficiency, C_0 is the absorption of the initial concentration when adsorption–desorption equilibrium was achieved, and C_t is the concentration at a certain irradiation time.

Hydroxyl radical detection

Coumarin can readily react with $\bullet\text{OH}$ to produce highly fluorescent product, 7-hydroxycoumarin (7HC) (umbelliferone) (Louti et al. 2005), as shown in Eq. 8. Therefore, the production of $\bullet\text{OH}$ on the surface of the light-illuminated PS@CdS CSNPs was detected by fluorescent probe method (Saif et al. 2012). The experimental procedure was similar to the measurement of photocatalytic activity except to coumarin (100 mL, 0.1 g/L) replaced RhB solution. During the experiments, aliquots were sampled at the given time intervals and centrifuged immediately. Then the supernatants were directly analyzed by the fluorescence spectrophotometer (Shanghai Lengguang Technology Co., Ltd., China, F97Pro) with the excitation wavelength at 340 nm.

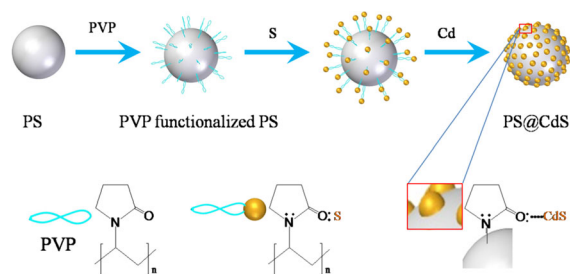


(8)

Results and discussion

Formation mechanism of PS@CdS CSNPs

A schematic diagram of the formation of PS@CdS CSNPs is illustrated in Scheme 1; monodisperse PS microspheres were synthesized firstly via emulsifier-free emulsion polymerization. As an amphiphilic and nonionic surfactant, the PVP with polar amine and carbonyl groups on one side and the nonpolar methylene groups on another side was introduced. PVP lacks acidic protons, but contains two electron-donating centers (the $-\text{C}=\text{O}$ group and the N atom of the pyrrole ring). The $-\text{C}=\text{O}$ group of PVP was considered to be the most favorable site for interaction due to the steric constraints on the N atom (Gupta et al. 2005). Thus, the nonpolar side of PVP directly bound to the polymer PS, whereas the $-\text{C}=\text{O}$ group of polar side can interact with S from TAA during ultrasonic, that is to say, PVP-functionalized PS microspheres offered



Scheme 1 Illustration of preparation of PS@CdS CSNPs

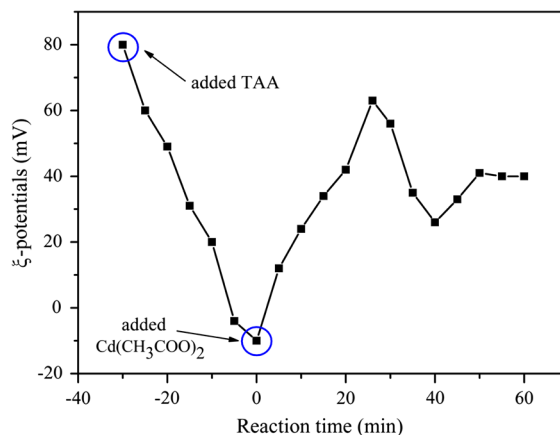


Fig. 1 ζ -potentials changed with the reaction time

anchor sites for S, therefore the reaction of Cd and S only occurred on the surface of PS microspheres. Once CdS nanoparticles were formed, it could act as a nucleating site for the further growth of CdS until forming uniform CdS coating. This was corroborated by Zeta potential analysis (Fig. 1). As TAA was added, the ζ -potentials decreased gradually. It indicated that the S atom from TAA adsorbed on the surface of PVP-functionalized PS microspheres. Upon the addition of $\text{Cd}(\text{CH}_3\text{COO})_2$, the increased ζ -potentials suggested CdS nucleating and growth. The CdS shell continued to thicken after 50 min; the ζ -potentials also achieved equilibrium. It should be pointed out that ultrasound-induced cavitation also played an important role in mixing the reactants and accelerating the release of S from TAA, which was necessary to form PS@CdS core/shell-type nanostructure (Gao et al. 2005; Ma et al. 2003).

In order to comprehensively understand the formation mechanism of PS@CdS CSNPs, it was essential to investigate the effects of experimental conditions on the formation of the hybrids. Hence, a variety of

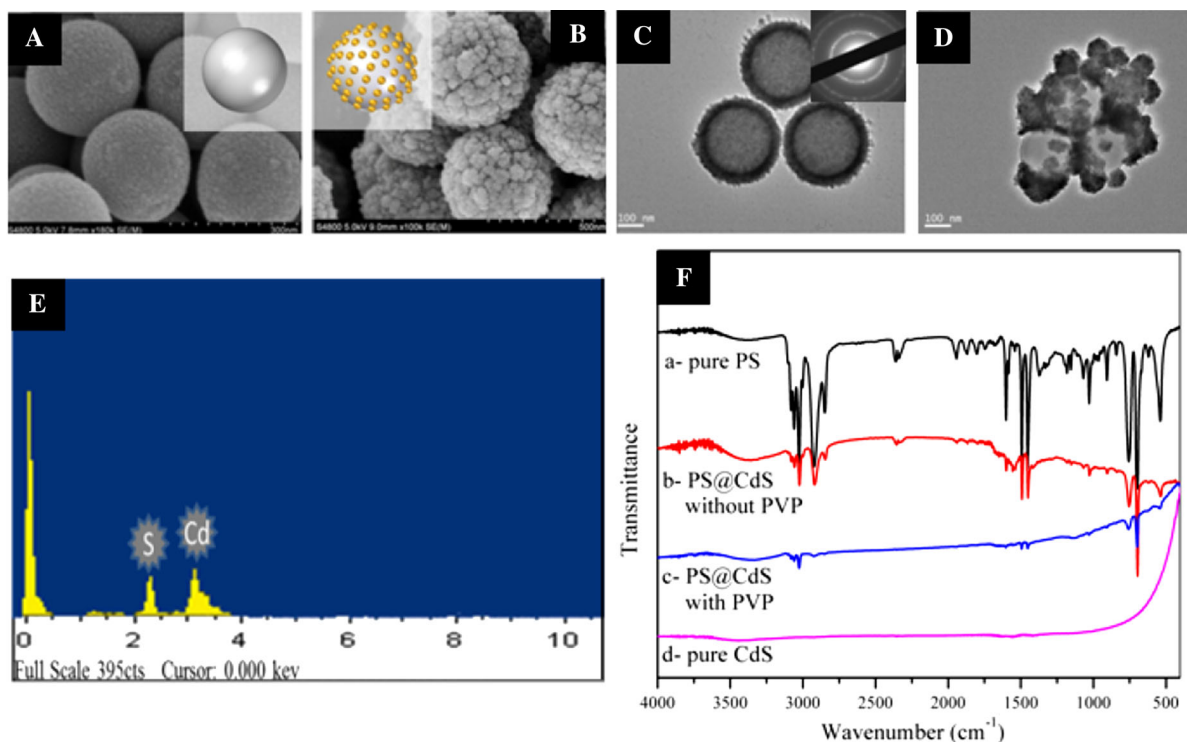


Fig. 2 SEM images of **a** bare PS NPs and **b** PS@CdS CSNPs (the *insets* of **a** and **b** are the corresponding model illustrations). TEM images of PS@CdS CSNPs and SAED pattern (*inset*) with

PVP (**c**), and without PVP (**d**), **e** EDS pattern of the shell of PS@CdS CSNPs and **f** FT-IR pattern of samples

reaction parameters such as PVP, the order of adding precursors, the molar ratio of S/Cd, as well as the reaction time were carefully examined.

Effect of PVP on samples structure

To analyze the role of the surfactant PVP in this strategy, a set of comparative experiments were performed. The typical SEM and TEM images of PS@CdS CSNPs prepared with and without PVP are demonstrated in Fig. 2. The virgin PS microspheres appeared as uniform smooth spherical particles with a diameter of ca. 260 nm (Fig. 2a). Compared with the original PS spheres, rougher surfaces were observed for all PS@CdS CSNPs as in Fig. 2b; the shell layer which seemed as a raspberry was composed of a large number of small and closely arranged CdS nanocrystallites. The clear core-shell structure was shown in Fig. 2c. The gray part was PS polymer core, while the dark part in stark contrast

was CdS shell. According to these images, the typical core-shell structure formed by this method consisted of a ca. 260 nm core and a uniform, continuous, and complete ca. 30 nm shell with good monodispersity. The SAED pattern (*inset* in Fig. 2c) demonstrated the detail of the local polycrystalline structure, and the concentric rings could be assigned as diffractions from the (111), (220), and (311) planes of face-centered cubic CdS, which was consistent with the latter XRD result. The EDS pattern of surface layer of as-prepared PS@CdS CSNPs was shown in Fig. 2e; high intensity peaks were found for S and Cd characteristic lines, which further confirmed the existence of CdS nanoparticles on the PS microspheres. The atomic ratio of S/Cd were found to be 50.4/49.6.

A control experimental result without PVP was shown in Fig. 2d. Only large amounts of CdS particles deposited randomly on the surface of PS microspheres and no continuous CdS shell was observed, which

might be due to the extensive growth and aggregation of pure CdS NPs. Typically, there was a large interfacial energy between a polymer and a Sulfide, mainly because of their lattice mismatch and lack of chemical interaction (Sun et al. 2013). When the PS–CdS interface was not improved, it was extremely difficult to form PS–CdS into complete core–shell structure (thermodynamically unfavorable). Yet the CdS self assembly should take low-energy pathways, which led to the aggregation of pure CdS NPs.

Figure 2f shows the FT-IR spectra of these samples. It indicated that polystyrene particles were formed after styrene polymerized (curve a): The peaks observed at 3,059 and 3,024 cm^{-1} were due to the stretching vibration of the aromatic C–H, while the absorption peaks at 2,922 and 2,848 cm^{-1} were due to the stretching vibration of the aliphatic C–H. Besides, the appearance of the band at 1,600 cm^{-1} was attributed to the stretching vibration of the skeleton of benzene ring, and the peak observed at 1,452 cm^{-1} was due to the bending vibration of the methylene. The absorption peaks at 756 and

697 cm^{-1} were due to the stretching vibration of the five adjacent C–H on the benzene ring. Obviously, the peaks observed at 539 cm^{-1} and 3,418 cm^{-1} were contributed by the distortion vibration of C=C of styrene and the stretching vibration of the O–H, respectively. For pure CdS (curve d), the vibrational absorption peak of the Cd–S bond, which should be at 405 cm^{-1} (Wu et al. 2004), cannot be observed, for it was rather weak and was scarcely resolved. However, in the curve of PS@CdS CSNPs (curve c), the absorption peaks of PS were completely covered by CdS within the range of 1,370–3,081 cm^{-1} , and the peaks in the ranges of 2,848–3,081, 1,372–1,600, and 539–756 cm^{-1} were significantly weakened, whereas peak at 3,418 cm^{-1} showed the stretching vibration of the O–H. This indicated that PS microspheres were coated with CdS, and PS@CdS CSNPs contained OH^- . But curve b was without PVP, all the absorption peaks of PS were only slightly weakened, this suggested that PS microspheres were not completely coated with CdS. These results again illustrated that PS@CdS

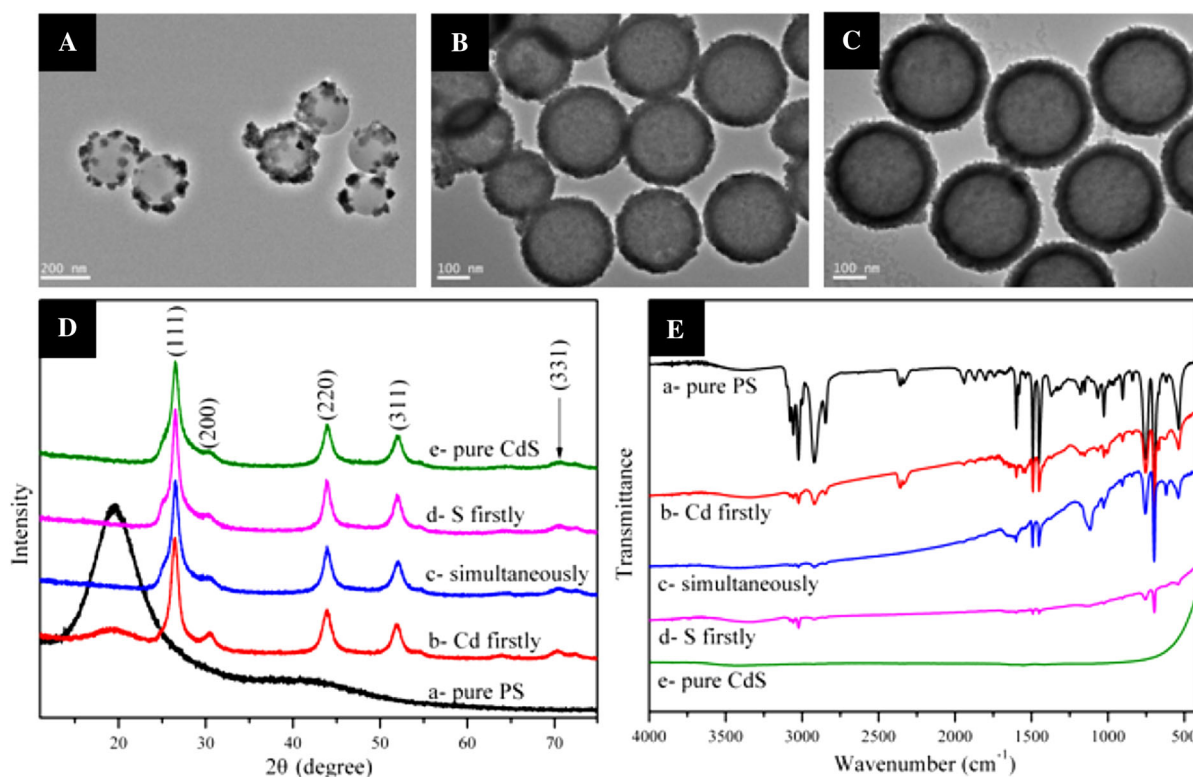


Fig. 3 TEM images of PS@CdS CSNPs **a** Cd first, **b** meantime added, **c** S first, **d** XRD, and **e** FT-IR patterns of samples

CSNPs were synthesized successfully due to the ability of PVP to bind the CdS and PS matrix.

Effect of the order of adding precursors on samples structure

To further demonstrate the superiority and efficiency of this experiment routine, we investigated the effect of the order of adding precursors on PS@CdS CSNPs. Because of the interaction of the nonpolar side of PVP with the surface of PS microspheres, the polar amine and carbonyl groups on the other side should bind either S or Cd by electrostatic interaction. However, only a few scattered CdS particles grew on the surface of PS microspheres for samples prepared by adding the Cd source firstly, as shown in Fig. 3a. This indicated that the polar carbonyl groups interact poorly with Cd due to the steric constraints on the N atom and fail to form core-shell structure. Interestingly, when the precursors of Cd and S were simultaneously added (Fig. 3b) or when the S source was introduced firstly (Fig. 3c), core-shell structure PS@CdS CSNPs were obtained in both cases. This result could be explained by formation mechanism of PS@CdS CSNPs in Scheme 1, in which S preferentially bonded to the $-C=O$ group in the polar side of PVP, Cd reacted with S, thereby leading to the formation of PS@CdS CSNPs with a uniform morphology and thin layer shell coating.

In addition, TEM observations of the different order of adding precursors confirmed that the complete degree of coated PS microspheres with CdS NPs, which was consistent with the results of XRD analysis (Fig. 3d) and FT-IR spectra (Fig. 3e). As demonstrated in Fig. 3d, amorphous PS showed a very broad diffraction peak at 2θ value of ca. 19° (curve a). For the Cd source firstly added (curve b), diffraction peaks at 2θ of 26.5° , 30.6° , 43.9° , 51.9° , and 70.5° assigned to the (111), (200), (220), (311), and (331) planes of cubic CdS crystal (JCPDC reference 06-0314) appeared, but the diffraction peak of PS was also observed, which suggested that the PS cores were not completely covered with CdS. For the sources of Cd and S simultaneously added (curve c) or the S source firstly added (curve d), almost all the diffraction peaks sample were same with curve b, on which only the peak of PS at 19° disappeared. This indicated that complete core-shell structure PS@CdS NPs were synthesized in both cases.

Figure 3e showed the FT-IR spectra of the corresponding samples, from curve a–d, the absorption peaks of PS were decreased in that order, which suggested the complete degree of coated PS microspheres with CdS NPs in the following order: S firstly > simultaneously added > Cd firstly.

Hence, both PVP and the order of adding precursors were found to be the main factors for PS@CdS CSNPs preparation, in which the surfactant PVP played a decisive role in the full CdS encapsulation of PVP-modified PS microsphere. (1) PVP stabilized colloidal particles such as PS microspheres in water, which can enhance the solubility of organic compounds (Graf et al. 2006; Gupta et al. 2005). (2) PVP can avoid effective aggregation of the CdS NPs, because the PVP-functionalized PS microspheres offered anchor sites for S from the release of TAA, leading to the nucleation of CdS particles around the sites, which was essential for the subsequent growth of complete and monodispersed PS@CdS core-shell structure nanohybrids during the reaction stage. (3) PVP has enhanced the bonding strength between CdS NPs and PS microspheres; this was due to the fact that methylene groups of PVP connected polymer via chemical bonds besides physical adsorption so as to reduce the PS–CdS interfacial energy (Sun et al. 2013), resulting in as-prepared PS@CdS CSNPs having higher mechanical strength.

Effect of the molar ratio of S/Cd on sample structures

The representative SEM images of PS@CdS samples obtained at different molar ratios of S/Cd are illustrated in Fig. 4. When the molar ratio of S/Cd was 1:1, only a few CdS particles grew on the surface of PS microspheres and the mean diameter of the hybrids spheres was about 265 nm (Fig. 4a). The corresponding EDS pattern of surface layer of as-prepared PS@CdS CSNPs is shown in Fig. 4d, which confirmed the existence of CdS NPs on the PS microspheres. It was obvious that C peak was caused by the grid. But O mainly derived from $-C=O$ group of PVP, attributing to not enough S to attach to the surface of PVP-functionalized PS microspheres during the synthesis of samples at lower S/Cd ratio of 1:1. This further indicated CdS particles coated with an incomplete package.

When the molar ratio increased to 1.4:1, the composite spheres appeared uniform, continuous,

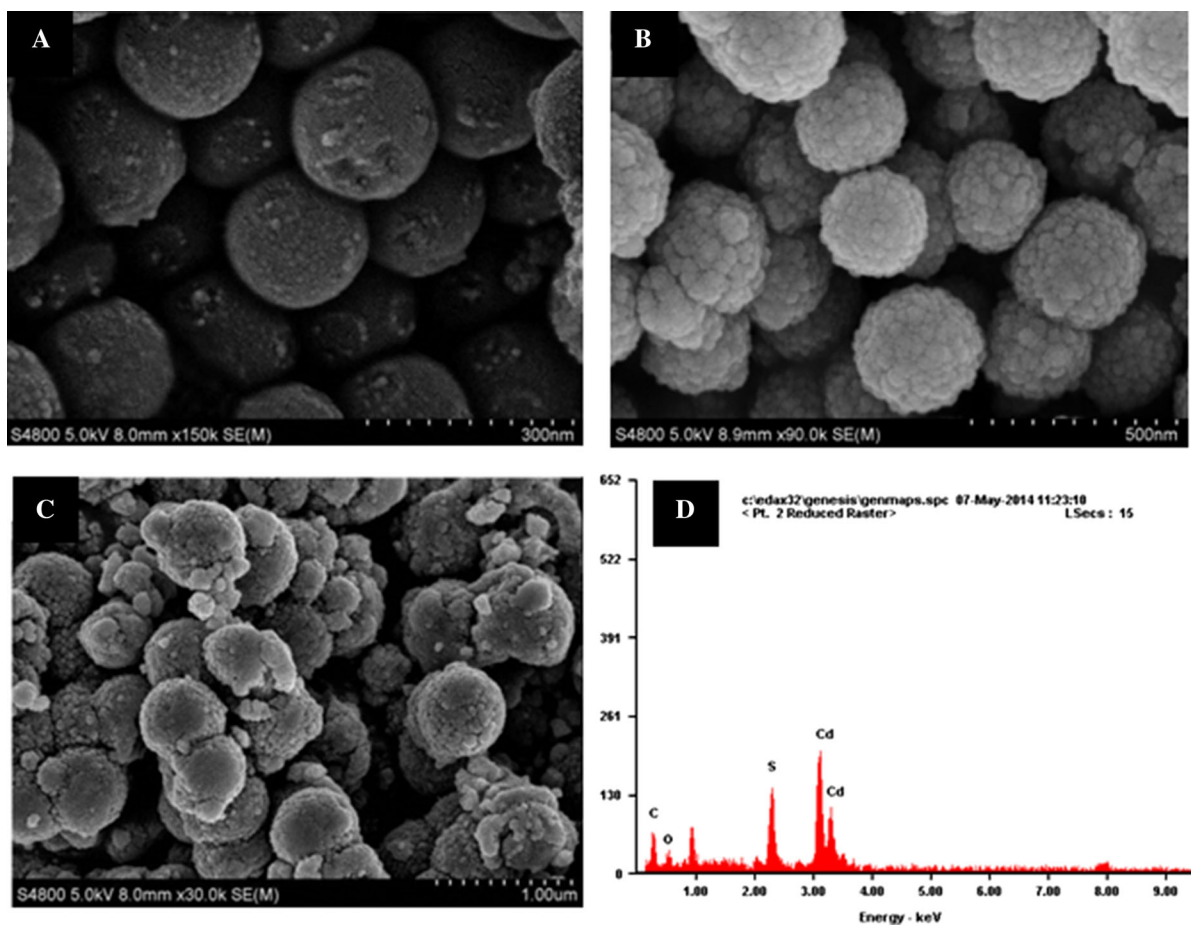


Fig. 4 SEM images of PS@CdS CSNPs prepared using S/Cd molar ratios of **a** 1:1, **b** 1.4:1, and **c** 2:1 and **d** EDS pattern of the shell of PS@CdS CSNPs at S/Cd molar ratio of 1:1

and integrated with diameters centralized at ca. 290 nm (Fig. 4b), which resulted in the formation of core-shell structure with an adequate molar ratio of S/Cd and the shell thickness was in a certain trend of escalation with the molar ratio of S/Cd. However, raising the molar ratio of S/Cd to 2:1, conglutination and agglomeration occurred, but no obvious change in the diameter of the hybrids was observed (Fig. 4c), which was probably because the PS microsphere surface could not provide enough anchor sites for S. As a result, a large amount of CdS particles grew freely in the peripheral when the concentration of S was more higher than that of Cd. Therefore, maintaining sufficient concentrations of reactants was important for forming core-shell composite.

The XRD results (Fig. 5) demonstrated the growth of the CdS nanocrystallites in the PS@CdS CSNPs. In

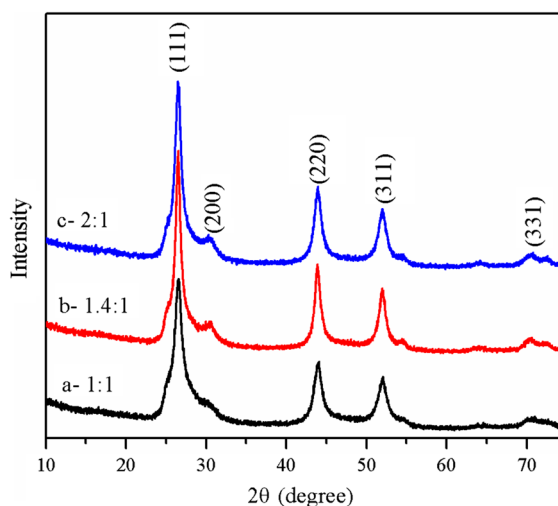


Fig. 5 XRD patterns of PS@CdS CSNPs of different molar ratios of S/Cd

the three cases of different molar ratios of S/Cd, the XRD patterns all exhibited high consistency, which were of pure cubic sphalerite type. The phenomena reflected that the CdS nanocrystallites in the PS@CdS CSNPs grew in the same way.

Effect of reaction time on samples structure

Figure 6 depicted the typical TEM images of PS@CdS samples synthesized at different reaction times. When the reaction time was 1.0 h, the CdS particles were distributed on the surface of PS microspheres in clusters, and the wall thickness was only 5–10 nm (Fig. 6a). When the growth time was 2 h, the coating was not smooth and the shell thickness was 10–15 nm (Fig. 6b), which might be probably due to the incomplete growth of CdS crystals. When reaction time went up to 3 h, not only the dispersion of PS@CdS was improved, but the core-shell structure was also formed with a smooth, complete, and continuous 20–30 nm shell as shown in Fig. 6c. This suggested that the growth of CdS nanocrystallite achieved stability and equilibrium. Nevertheless, when reacting time was 4 h, the shell layer stopped thickening; agglomeration and conglutination among

microspheres took place and the dispersibility of PS@CdS CSNPs was poor (Fig. 6d). This result suggested that the shell thickness of PS@CdS CSNPs increased with the increasing time in certain range, and it could be adjusted by altering reaction time. As the time was more than 4 h, the overgrowth of CdS crystals tended to aggregate together on PS@CdS CSNPs to a certain extent.

Figure 7a–d show the XRD patterns for the products obtained at different reaction times from 1 to 4 h, which showed that the diffraction peaks for the CdS indexed to pure cubic phase increased with increasing time. These results indicated that both the CdS nanocrystallite sizes and the CdS contents in the composites increase with increasing time. This further indicated that the growth of the CdS nanocrystallites in the PS@CdS CSNPs agreed with the aforementioned formation mechanism of PS@CdS CSNPs.

UV–Vis DRS spectra

The UV–Vis DRS spectra of CdS and PS@CdS CSNPs are shown in Fig. 8. A strong absorption in the visible light region can be assigned to the intrinsic bandgap absorption of CdS. In addition, a red-shift

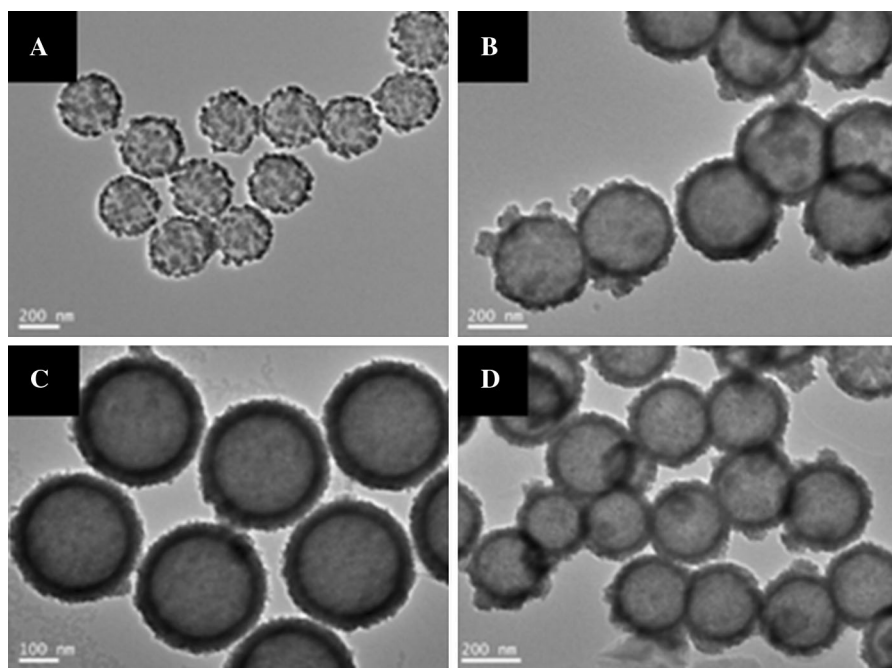


Fig. 6 TEM images of PS@CdS CSNPs in different reaction times: **a** 1.0 h, **b** 2 h, **c** 3 h, and **d** 4 h

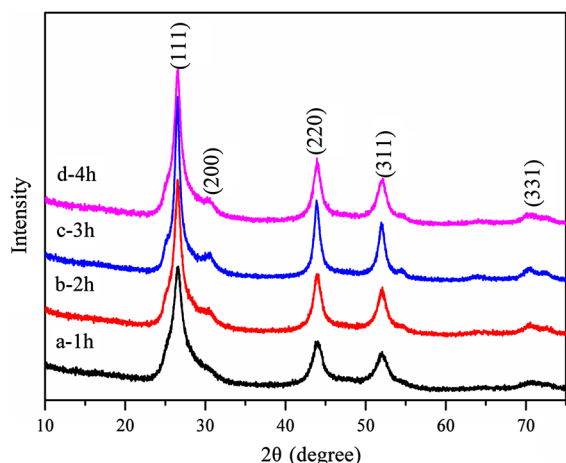


Fig. 7 XRD patterns of PS@CdS CSNPs at different reaction times

for PS@CdS CSNPs was observed, which might suggest that there was a decrease in energy band gap of these samples. The direct band gap values of the CdS and PS@CdS samples were estimated from the $(\alpha hv)^2$ versus photon energy ($h\nu$) plot as shown in the inset of Fig. 8. The band gaps of the PS@CdS samples were estimated to be 2.15 eV, which was lower than that of CdS (2.16 eV). The above results showed that the absorption spectrum was broadened and the band gap was narrowed by building a core-shell structure of PS@CdS CSNPs. This wider absorption edge in the visible light region than that of CdS indicated that this sample had greater carrier concentration, since the optical absorption in this wavelength region was due to free carrier absorption of the conduction electrons. Therefore, PS@CdS CSNPs might have higher visible light-driven photocatalytic activity than pure CdS.

Photocatalytic degradation of RhB

The data in Fig. 9a, b display the photodegradation behaviors of RhB catalyzed by PS@CdS CSNPs and pure CdS NPs under visible light illumination, respectively. The absorption bands of RhB showed two types of spectral changes. One was a hypsochromic shift in the absorbance maximum, and the other was a decrease in absorbance. Moreover, absorption peaks located at wavelengths lower than 400 nm also decreased rapidly during the illumination period. The gradual hypsochromic shifts of the absorption

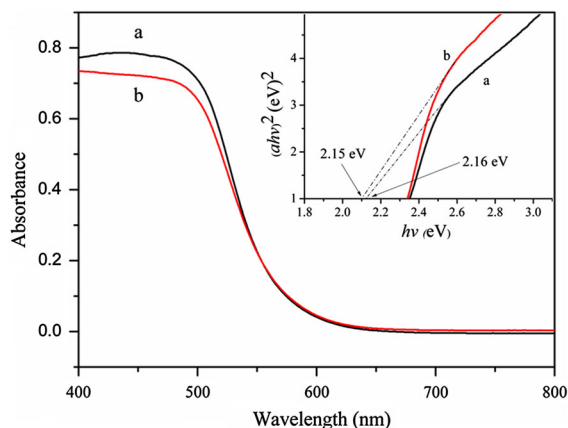


Fig. 8 UV-Vis DRS of **a** pure CdS **b** PS@CdS CSNPs. The inset shows band gap evaluation from the plots of $(\alpha hv)^2$ versus photon energy ($h\nu$)

maximum were caused by the *N*-deethylation of RhB during irradiation, whereas the characteristic absorption of RhB around 554 nm decreased, indicating that the cleavage of the conjugated chromophore structure occurred simultaneously (Horikoshi et al. 2003; Hu et al. 2006). This indicated both PS@CdS CSNPs and pure CdS have a good photocatalytic activity.

Figure 10 summarizes the corresponding wavelength shifts and the decolorization efficiency in the major absorption bands of the RhB solution. As shown in Fig. 10, a similar tendency can be found in the spectral changes in RhB over both PS@CdS CSNPs and pure CdS. But both wavelength shifts and the decolorization efficiency for PS@CdS CSNPs were faster than pure CdS. Regardless of visible light irradiation, the decolorization efficiency of RhB over PS@CdS CSNPs was up to 92.67 %, and wavelength shifted from 554 to 526 nm within 70 min. For pure CdS, the decolorization efficiency was only 80.86 % and a blue shift of the band to 530 nm. From these results, we concluded that the photocatalytic activity of PS@CdS CSNPs was enhanced compared to the pure CdS. The enhanced photocatalytic activity of PS@CdS CSNPs can be achieved through the following possible reasons. The first was PVP effectively improve the dispersion stability of the PS@CdS CSNPs in water. Second, the hydroxyl groups of PS microsphere surfaces may accept photogenerated holes to prevent electron-hole recombination (Zabek et al. 2009). The separation of photogenerated electron-holes can significantly

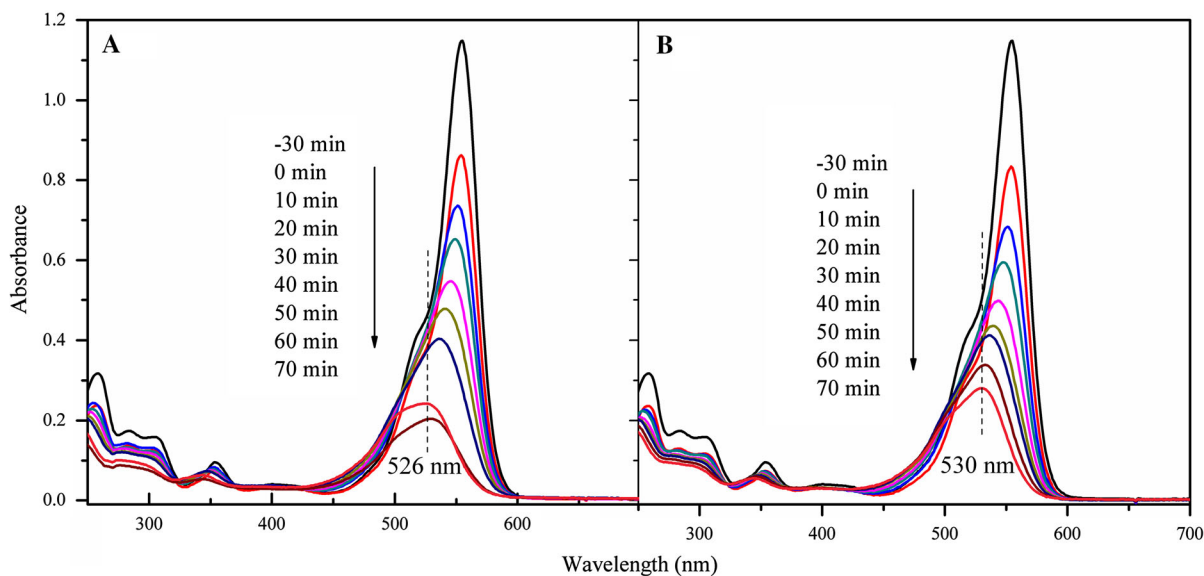


Fig. 9 Temporal changes in the absorption spectra patterns during the photocatalyzed degradation of RhB solution (2 mM) under visible light irradiation: **a** PS@CdS CSNPs **b** pure CdS

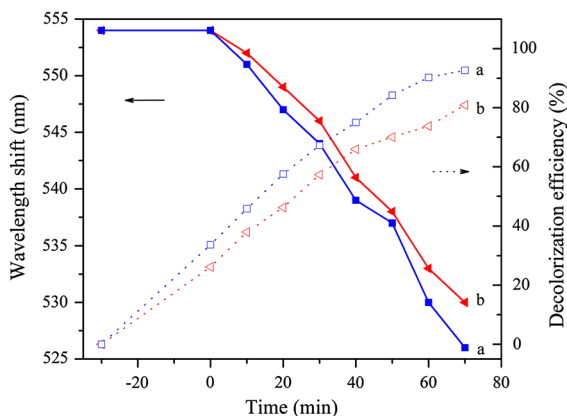


Fig. 10 Maximum absorption wavelength shifts (*line*) and decolorization efficiency (*dotted line*) of RhB as a function of reaction time under visible light irradiation over *a* PS@CdS CSNPs and *b* pure CdS

be facilitated in the presence of PS core. Furthermore, the pollutants RhB were adsorbed on adsorbent supports (PS spheres), resulting in a higher pollutant environment around the loaded CdS nanoparticles (Hu et al. 2010). The third was attributed to the stabilizing CdS from PVP, while pure CdS was easy to occur photo-corrosion to some extent, which led to the more efficient mass of PS@CdS CSNPs than pure CdS. In

addition, PS@CdS CSNPs surface contained amount of OH^- , as given by FT-IR analysis in Fig. 2f (curve c). On the one hand, OH^- was beneficial to absorb RhB molecules, on the other hand, OH^- promoted to produce $\cdot\text{OH}$ (Eqs. 1, 3).

The stability of a photocatalyst is important to its application. The durability of PS@CdS CSNPs was tested by RhB degradation for five recycles under visible light irradiation. As shown in Fig. 11, the catalyst can decolorize RhB dye efficiently without significant deactivation after five-time recycling. The results showed that the photocatalytic activity of PS@CdS CSNPs has a good stability.

Analysis of hydroxyl radicals and primary active species

Figure 12 shows the typical PL spectral changes observed during visible light irradiation in the system of PS@CdS CSNPs and coumarin. It was clearly seen that the PL intensity of photogenerated 7-hydroxycoumarin at about 453 nm (Loutit et al. 2005) (excited at 340 nm) increased with the irradiation time, which was similar to the RhB decolorization efficiency from PS@CdS CSNPs (Fig. 9a). This result indicated that the fast

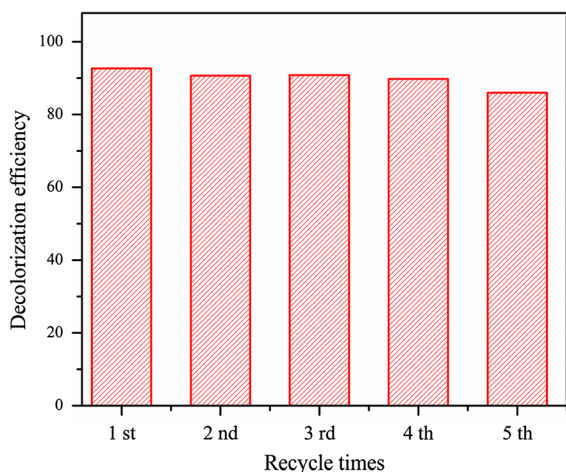


Fig. 11 Decolorization efficiency of RhB with PS@CdS CSNPs under visible light irradiation after 70 min

production of OH radicals and the highly accumulated OH radicals might be the main active oxygen species in the photocatalytic process.

It was generally accepted that the photocatalytic degradation of organic compounds proceeds via two routes: direct hole (h^+) oxidation or \bullet OH oxidation. Isopropanol, which acts as an efficient \bullet OH scavenger (Chen et al. 2005), was added to the solutions at the beginning of the photocatalytic reaction to quench \bullet OH in the irradiated PS@CdS CSNPs samples. Figure 13 exhibited the temporal adsorption spectral changes of RhB solution with isopropanol addition (10 mM) under visible light irradiation. As shown in Fig. 13, the absorbance of RhB decreases quickly in darkness, which can be achieved through physicochemical adsorption of PS@CdS CSNPs. However, remarkable inhibitory effect was observed after irradiation. Moreover, absorption peaks located at wavelengths lower than 400 nm also remain unchanged during the illumination period. The isopropanol quenching result suggested that \bullet OH played an essential role in the reaction mechanism of RhB oxidation. Despite all this, the degradation of RhB to some extent can still be observed. The result indicated that photocatalytic degradation of RhB mainly came from \bullet OH, whereas the rest were from h^+ . With this viewpoint, the higher degradation efficiency of RhB in the PS@CdS CSNPs system can be attributed to the higher concentration and generation rate of \bullet OH in homogeneous media.

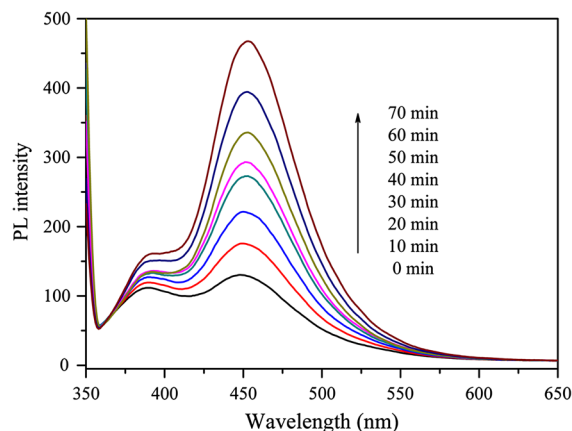


Fig. 12 PL intensities of COU reaction solutions in the presence of PS@CdS CSNPs under visible light irradiation. Excitation wavelength was 340 nm

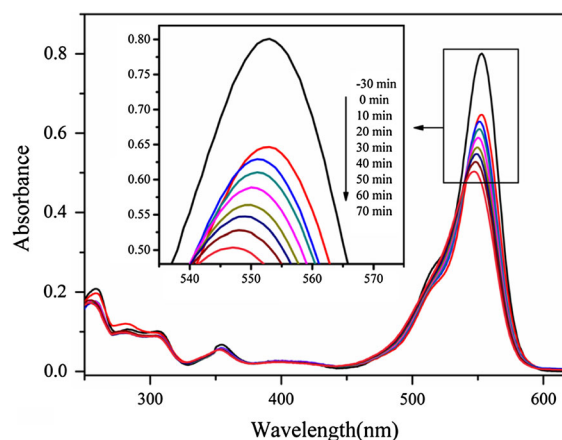
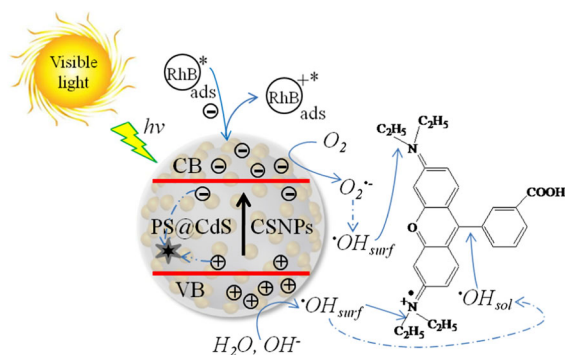


Fig. 13 Effect of isopropanol addition (10 mM) in the photocatalyzed degradation of RhB (2 μ M) with irradiated PS@CdS CSNPs

Degradation mechanism of RhB over PS@CdS CSNPs

On the basis of the above explanations for the photoinduced degradation of RhB over the PS@CdS CSNPs, the proposed photochemical processes are elucidated in Scheme 2. The PS@CdS CSNPs can be excited to produce electron-hole pairs; part of the charge carriers rapidly underwent recombination. But when RhB molecules were chemisorbed onto PS@CdS CSNPs and excited, they could inject electrons into the conduction band of PS@CdS



Scheme 2 Degradation mechanism of RhB over PS@CdS CSNPs

CSNPs. The electrons can be captured by the oxygen in solution to yield oxidant $\cdot\text{OH}$ (Eqs. 4–6). The valence band h^+ were subsequently trapped by the surface bound OH^- (or by H_2O) to yield $\cdot\text{OH}$ (Eqs. 2, 3). Based on the document (Turchi and Ollis 1990; Wu et al. 1998; Xing et al. 2014), $\cdot\text{OH}$ can exist in one of the two basic forms in homogeneous system. One was at the surface of the catalyst ($\cdot\text{OH}_{\text{surf}}$) and another was in the bulk solution ($\cdot\text{OH}_{\text{sol}}$). During the initial irradiation period, the $\cdot\text{OH}_{\text{surf}}$ can attack the diethylamino groups effectively. With the ceaseless formation of $\cdot\text{OH}_{\text{surf}}$, $\cdot\text{OH}$ may diffuse into the bulk solution ($\cdot\text{OH}_{\text{sol}}$) and then attack the chromophoric structure, leading to the cycloreversion of the RhB compounds (Turchi and Ollis 1990; Wu et al. 1998). Therefore, it was reasonable to think that N-deethylation and cycloreversion of RhB occurred in the photocatalytic process of RhB over PS@CdS CSNPs.

Conclusions

In summary, we successfully synthesized PS@CdS CSNPs via a simple sonochemical method. Both PVP and the order of adding precursors were found to be the controlling parameters. The as-prepared nanohybrids have a typical core-shell structure with 260 nm core and a uniform shell with thickness ranging from 10 to 30 nm. Furthermore, their shell thickness could be controlled by adjusting preparation conditions, such as the molar ratio of S/Cd and the reaction time. Photocatalytic degradation of RhB indicated that the photocatalytic activity of PS@CdS CSNPs under visible light irradiation was enhanced compared to the pure CdS, which should be attributed to the synergic effect

between the core and the shell, amount of hydroxyl groups on the surface, good monodispersity, and so on. In addition, this catalyst showed improved stability, and the activity did not decrease significantly after fifth recycle. Furthermore, hydroxyl radical detection and isopropanol quenching method suggested $\cdot\text{OH}$ was the main active oxygen species in the photocatalytic process. Our research not only broadens the application of sonochemical method, but also provides operability for synthesis of hollow CdS materials, single core double shells or single core multi shells, and expands the research and application scope of the CdS core-shell nanomaterials.

Acknowledgments This work is financially supported by the National Natural Science Foundation of China (Grant No. 21176260 and 21376268), Taishan Scholar Foundation (No. ts20130929) and the National Basic Research Program of China (No. 2011CB605703).

References

- Anandan S, Grieser F, Ashokkumar M (2008) Sonochemical synthesis of Au–Ag core–shell bimetallic nanoparticles. *J Phys Chem C* 112(39):15102–15105. doi:[10.1021/jp806960r](https://doi.org/10.1021/jp806960r)
- Bang JH, Suslick KS (2010) Applications of ultrasound to the synthesis of nanostructured materials. *Adv Mater* 22(10):1039–1059. doi:[10.1002/adma.200904093](https://doi.org/10.1002/adma.200904093)
- Breen ML, Dinsmore AD, Pink RH, Qadri SB, Ratna BR (2001) Sonochemically produced ZnS-coated polystyrene core-shell particles for use in photonic crystals. *Langmuir* 17(3):903–907. doi:[10.1021/la0011578](https://doi.org/10.1021/la0011578)
- Caruso F (2001) Nanoengineering of particle surfaces. *Adv Mater* 13(1):11–22. doi:[10.1002/1521-4095\(200101\)13:1<11:AID-ADMA11>3.0.CO;2-N](https://doi.org/10.1002/1521-4095(200101)13:1<11:AID-ADMA11>3.0.CO;2-N)
- Chen Y, Yang S, Wang K, Lou L (2005) Role of primary active species and TiO_2 surface characteristic in UV-illuminated photodegradation of acid orange 7. *J Photochem Photobiol A* 172(1):47–54. doi:[10.1016/j.jphotochem.2004.11.006](https://doi.org/10.1016/j.jphotochem.2004.11.006)
- Coşkun M, Korkmaz M (2014) The effect of SiO_2 shell thickness on the magnetic properties of ZnFe_2O_4 nanoparticles. *J Nanopart Res* 16(3):1–12. doi:[10.1007/s11051-014-2316-3](https://doi.org/10.1007/s11051-014-2316-3)
- Douvalis A, Zboril R, Bourlinos A, Tucek J, Spyridi S, Bakas T (2012) A facile synthetic route toward air-stable magnetic nanoalloys with Fe–Ni/Fe–Co core and iron oxide shell. *J Nanopart Res* 14(9):1–16. doi:[10.1007/s11051-012-1130-z](https://doi.org/10.1007/s11051-012-1130-z)
- Fang FF, Kim JH, Choi HJ (2009) Synthesis of core-shell structured PS/ Fe_3O_4 microbeads and their magnetorheology. *Polymer* 50(10):2290–2293. doi:[10.1016/j.polymer.2009.03.023](https://doi.org/10.1016/j.polymer.2009.03.023)
- Gao T, Li Q, Wang T (2005) Sonochemical synthesis, optical properties, and electrical properties of core/shell-type ZnO

- nanorod/CdS nanoparticle composites. *Chem Mater* 17(4):887–892. doi:10.1021/cm0485456
- Geng J, Jia X-D, Zhu J-J (2011) Sonochemical selective synthesis of ZnO/CdS core/shell nanostructures and their optical properties. *CrystEngComm* 13(1):193–198. doi:10.1039/C0CE00180E
- Ghosh Chaudhuri R, Paria S (2011) Core/shell nanoparticles: classes, properties, synthesis mechanisms, characterization, and applications. *Chem Rev* 112(4):2373–2433. doi:10.1021/cr100449n
- Graf C, Dembski S, Hofmann A, Rühl E (2006) A general method for the controlled embedding of nanoparticles in silica colloids. *Langmuir* 22(13):5604–5610. doi:10.1021/la060136w
- Gupta P, Thilagavathi R, Chakraborti AK, Bansal AK (2005) Role of molecular interaction in stability of celecoxib–PVP amorphous systems. *Mol Pharm* 2(5):384–391. doi:10.1021/mp050004g
- Horikoshi S, Saitou A, Hidaka H, Serpone N (2003) Environmental remediation by an integrated microwave/UV illumination method. V. Thermal and nonthermal effects of microwave radiation on the photocatalyst and on the photodegradation of rhodamine-B under UV/Vis radiation. *Environ Sci Technol* 37(24):5813–5822. doi:10.1021/es030326i
- Hu X, Mohamood T, Ma W, Chen C, Zhao J (2006) Oxidative decomposition of rhodamine B dye in the presence of VO_2^+ and/or Pt(IV) under visible light irradiation: N-deethylation, chromophore cleavage, and mineralization. *J Phys Chem B* 110(51):26012–26018. doi:10.1021/jp063588q
- Hu Y, Liu Y, Qian H, Li Z, Chen J (2010) Coating colloidal carbon spheres with CdS nanoparticles: microwave-assisted synthesis and enhanced photocatalytic activity. *Langmuir* 26(23):18570–18575. doi:10.1021/la103191y
- Huang KJ, Rajendran P, Liddell CM (2007) Chemical bath deposition synthesis of sub-micron ZnS-coated polystyrene. *J Colloid Interface Sci* 308(1):112–120. doi:10.1016/j.jcis.2006.11.057
- Imhof A (2001) Preparation and characterization of titania-coated polystyrene spheres and hollow titania shells. *Langmuir* 17(12):3579–3585. doi:10.1021/la001604j
- Ishibashi K-i, Fujishima A, Watanabe T, Hashimoto K (2000a) Detection of active oxidative species in TiO_2 photocatalysis using the fluorescence technique. *Electrochem Commun* 2(3):207–210. doi:10.1016/S1388-2481(00)00006-0
- Ishibashi K-i, Fujishima A, Watanabe T, Hashimoto K (2000b) Quantum yields of active oxidative species formed on TiO_2 photocatalyst. *J Photochem Photobiol A* 134(1–2):139–142. doi:10.1016/S1010-6030(00)00264-1
- Kandula S, Jeevanandam P (2014) Visible-light-induced photodegradation of methylene blue using ZnO/CdS hetero-nanostructures synthesized through a novel thermal decomposition approach. *J Nanopart Res* 16(6):1–18. doi:10.1007/s11051-014-2452-9
- Karabacak RB, Erdem M, Yurdakal S, Çimen Y, Türk H (2014) Facile two-step preparation of polystyrene/anatase TiO_2 core/shell colloidal particles and their potential use as an oxidation photocatalyst. *Mater Chem Phys* 144(3):498–504. doi:10.1016/j.matchemphys.2014.01.026
- Kim TH, Lee KH, Kwon YK (2006) Monodisperse hollow titania nanospheres prepared using a cationic colloidal template. *J Colloid Interface Sci* 304(2):370–377. doi:10.1016/j.jcis.2006.08.059
- Li S, Zheng J, Yang W, Zhao Y (2007) A new synthesis process and characterization of three-dimensionally ordered macroporous ZrO_2 . *Mater Lett* 61(26):4784–4786. doi:10.1016/j.matlet.2007.03.033
- Louit G, Foley S, Cabillic J, Coffigny H, Taran F, Valleix A, Renault JP, Pin S (2005) The reaction of coumarin with the OH radical revisited: hydroxylation product analysis determined by fluorescence and chromatography. *Radiat Phys Chem* 72(2–3):119–124. doi:10.1016/j.radphyschem.2004.09.007
- Ma Y, Qi L, Ma J, Cheng H, Shen W (2003) Synthesis of sub-micrometer-sized CdS hollow spheres in aqueous solutions of a triblock copolymer. *Langmuir* 19(21):9079–9085. doi:10.1021/la034994t
- Mizukoshi Y, Fujimoto T, Nagata Y, Oshima R, Maeda Y (2000) Characterization and catalytic activity of core–shell structured gold/palladium bimetallic nanoparticles synthesized by the sonochemical method. *J Phys Chem B* 104(25):6028–6032. doi:10.1021/jp994255e
- Monteiro OC, Esteves ACC, Trindade T (2002) The synthesis of SiO_2 @CdS nanocomposites using single-molecule precursors. *Chem Mater* 14(7):2900–2904. doi:10.1021/cm011257e
- Morel A-L, Nikitenko SI, Gionnet K, Wattiaux A, Lai-Kee-Him J, Labrugere C, Chevalier B, Deleris G, Petibois C, Brisson A, Simonoff M (2008) Sonochemical approach to the synthesis of Fe_3O_4 @ SiO_2 core–shell nanoparticles with tunable properties. *ACS Nano* 2(5):847–856. doi:10.1021/nl800091q
- Mu W, Fu M (2012) Synthesis of non-rigid core–shell structured PS/ SiO_2 composite abrasives and their oxide CMP performance. *Microelectron Eng* 96:51–55. doi:10.1016/j.mee.2012.02.047
- Murcia MJ, Shaw DL, Woodruff H, Naumann CA, Young BA, Long EC (2006) Facile sonochemical synthesis of highly luminescent ZnS–shelled CdSe quantum dots. *Chem Mater* 18(9):2219–2225. doi:10.1021/cm0505547
- Radmilovic V, Ophus C, Marquis EA, Rossell MD, Tolley A, Gautam A, Asta M, Dahmen U (2011) Highly monodisperse core–shell particles created by solid-state reactions. *Nat Mater* 10(9):710–715. doi:10.1038/nmat3077
- Rauf MA, Ashraf SS (2009) Fundamental principles and application of heterogeneous photocatalytic degradation of dyes in solution. *Chem Eng J* 151(1–3):10–18. doi:10.1016/j.cej.2009.02.026
- Rogach A, Susha A, Caruso F, Sukhorukov G, Kornowski A, Kershaw S, Möhwald H, Eychmüller A, Weller H (2000) Nano- and microengineering: 3-D colloidal photonic crystals prepared from sub- μm -sized polystyrene latex spheres pre-coated with luminescent polyelectrolyte/nanocrystal shells. *Adv Mater* 12(5):333–337. doi:10.1002/(SICI)1521-4095(200003)12:5<333:AID-ADMA333>3.0.CO;2-X
- Saif M, Aboul-Fotouh SMK, El-Molla SA, Ibrahim MM, Ismail LFM (2012) Improvement of the structural, morphology, and optical properties of TiO_2 for solar treatment of industrial wastewater. *J Nanopart Res* 14(11):1–11. doi:10.1007/s11051-012-1227-4

- Sanchez C, Julian B, Belleville P, Popall M (2005) Applications of hybrid organic-inorganic nanocomposites. *J Mater Chem* 15(35–36):3559–3592. doi:[10.1039/B509097K](https://doi.org/10.1039/B509097K)
- Shenoy DB, Antipov AA, Sukhorukov GB, Möhwald H (2003) Layer-by-layer engineering of biocompatible, decomposable core-shell structures. *Biomacromolecules* 4(2):265–272. doi:[10.1021/bm025661y](https://doi.org/10.1021/bm025661y)
- Sherman RL, Ford WT (2005) Semiconductor nanoparticle/polystyrene latex composite materials. *Langmuir* 21(11):5218–5222. doi:[10.1021/la0468139](https://doi.org/10.1021/la0468139)
- Shi F, Li Y, Wang H, Zhang Q (2012) Formation of core/shell structured polystyrene/anatase TiO₂ photocatalyst via vapor phase hydrolysis. *Appl Catal B* 123–124:127–133. doi:[10.1016/j.apcatb.2012.04.032](https://doi.org/10.1016/j.apcatb.2012.04.032)
- Siva C, Ramya R, Baraneedharan P, Nehru K, Sivakumar M (2014) Fabrication, physiochemical and optoelectronic characterization of SiO₂/CdS core-shell nanostructures. *J Mater Sci* 25(3):1202–1208. doi:[10.1007/s10854-014-1710-z](https://doi.org/10.1007/s10854-014-1710-z)
- Sun H, He J, Wang J, Zhang S-Y, Liu C, Sritharan T, Mhaisalkar S, Han M-Y, Wang D, Chen H (2013) Investigating the multiple roles of polyvinylpyrrolidone for a general methodology of oxide encapsulation. *JACS* 135(24):9099–9110. doi:[10.1021/ja4035335](https://doi.org/10.1021/ja4035335)
- Turchi CS, Ollis DF (1990) Photocatalytic degradation of organic water contaminants: mechanisms involving hydroxyl radical attack. *J Catal* 122(1):178–192. doi:[10.1016/0021-9517\(90\)90269-P](https://doi.org/10.1016/0021-9517(90)90269-P)
- Virtudazo RR, Watanabe H, Shirai T, Fuji M (2013) Simple preparation and initial characterization of semi-amorphous hollow calcium silicate hydrate nanoparticles by ammonia-hydrothermal-template techniques. *J Nanopart Res* 15(5):1–9. doi:[10.1007/s11051-013-1604-7](https://doi.org/10.1007/s11051-013-1604-7)
- Wang Y, Wang G, Wang H, Tang C, Jiang Z, Zhang L (2007) Microwave-assisted fabrication of PS@CdS core-shell nanostructures and CdS hollow spheres. *Chem Lett* 36(5):674–675. doi:[10.1246/cl.2007.674](https://doi.org/10.1246/cl.2007.674)
- Wang Z, Gao Y, Wang J-Y, Zhang J-H, Yang B (2008) Fabrication of CdS-nanoparticle/polystyrene latex through the combined use of surface-initiated ATRP and gas/solid reaction. *Chem J Chin Univ* 7: 1452–1455. <http://www.cqvip.com/qk/90335x/200807/27899069.html>
- Wu T, Liu G, Zhao J, Hidaka H, Serpone N (1998) Photoassisted degradation of dye pollutants. V. Self-photosensitized oxidative transformation of rhodamine B under visible light irradiation in aqueous TiO₂ dispersions. *J Phys Chem B* 102(30):5845–5851. doi:[10.1021/jp980922c](https://doi.org/10.1021/jp980922c)
- Wu D, Ge X, Zhang Z, Wang M, Zhang S (2004) Novel one-step route for synthesizing CdS/polystyrene nanocomposite hollow spheres. *Langmuir* 20(13):5192–5195. doi:[10.1021/la049405d](https://doi.org/10.1021/la049405d)
- Xing L, Xie Y, Cao H, Minakata D, Zhang Y, Crittenden JC (2014) Activated carbon-enhanced ozonation of oxalate attributed to HO oxidation in bulk solution and surface oxidation: effects of the type and number of basic sites. *Chem Eng J* 245:71–79. doi:[10.1016/j.cej.2014.01.104](https://doi.org/10.1016/j.cej.2014.01.104)
- Yin J, Qian X, Yin J, Shi M, Zhou G (2003) Preparation of ZnS/PS microspheres and ZnS hollow shells. *Mater Lett* 57(24–25):3859–3863. doi:[10.1016/S0167-577X\(03\)00217-9](https://doi.org/10.1016/S0167-577X(03)00217-9)
- Zabek P, Eberl J, Kisch H (2009) On the origin of visible light activity in carbon-modified titania. *Photochem Photobiol Sci* 8(2):264–269. doi:[10.1039/B812798K](https://doi.org/10.1039/B812798K)
- Zhang S, Zhu Y, Yang X, Li C (2005) Fabrication of core-shell latex spheres with CdS/polyelectrolyte composite multilayers. *Colloids Surf A* 264(1–3):215–218. doi:[10.1016/j.colsurfa.2005.03.024](https://doi.org/10.1016/j.colsurfa.2005.03.024)
- Zhang J, Tang Y, Lee K, Ouyang M (2010) Nonepitaxial growth of hybrid core-shell nanostructures with large lattice mismatches. *Science* 327(5973):1634–1638. doi:[10.1126/science.1184769](https://doi.org/10.1126/science.1184769)